Chapter 9
RF Impairments in MIMO Transceivers

Direct conversion transceivers are very attractive in wireless communications, due to their simplicity and ease of integration. However, their performances are degraded with radio frequency (RF) impairments. On the other hand, multiple input multiple output (MIMO) wireless communication systems promise higher spectral efficiency than what is possible with single input single output (SISO) wireless communications [1], [2]. However, the significant improvement in wireless system performance using MIMO is achieved by increasing the system complexity, which may result in higher sensitivity and lower performance in practical systems. Therefore, the degradations due to system impairments must be studied to evaluate the realistic behavior of the MIMO systems. Moreover, compensation techniques can be applied by understanding the effects of these impairment factors. These impairments may be noticed as phase noise, DC offset, in-phase / quadrature (I/Q) imbalance, and power amplifier nonlinearity [3]. In this chapter, the impairments due to phase noise, DC offset and I/Q imbalance are analyzed and the different techniques for their prevention and compensation are discussed. The power amplifier nonlinearity effects are investigated in the following chapter.

9.1 Phase Noise in MIMO Transceivers

Among various RF impairment factors, phase noise is one of the major sources of performance reduction in wireless communications systems. This section is mainly focused on the characterization and evaluation of phase noise effects on MIMO systems. By modeling the performance degradation due to the phase noise, a clear understanding of the system and compensation techniques are provided. On the other hand, by providing analytical relations to model the phase noise effects, the performance can be evaluated without the requirement of conducting very time-consuming simulation studies.

9.1.1 Phase Noise Model

Two types of phase noise models exist. When the system is phase locked, the resulting phase noise is low; and, it is modeled as a zero-mean, stationary, finite-power

A. Mohammadi et al.: RF Transceiver Design for MIMO Wireless Communications, LNEE 145, pp. 227–263.
springerlink.com

random process [4]. On the other hand, when the system is only frequency locked, the resulting phase noise slowly varies, but is not limited; and, it is modeled as a zero-mean, non-stationary, infinite-power Wiener process [5]. We assume the system employs a phase-locked loop (PLL) for its local oscillators (LO); hence, we use the first model. For simplicity, it is assumed for simplicity that the phase noise (θ_n), is a zero-mean Gaussian distributed random variable [6], [7]:

$$f_{\Theta_n}(\theta_n) = \frac{1}{\sqrt{2\pi}\sigma_{\theta_n}} e^{\frac{-\theta_n^2}{2\sigma_{\theta_n}^2}} \tag{9.1}$$

where $\sigma_{\theta_n}^2$ is the phase noise power.

In the first step, we extract the bit error rate (BER) of a SISO system with phase noise. If a SISO system has phase noise in the receiver, the received signal is expressed as:

$$r = ha_k e^{j\theta_n} + w \tag{9.2}$$

where r is the received signal, h denotes the channel gain, a_k is the transmitted symbol, θ_n is the random phase caused by the phase noise, and w is the additive white Gaussian noise (AWGN), which is a statistically independent and identically distributed (i.i.d.) complex-valued Gaussian random variable with a variance of N_0. It is assumed that h is a complex random variable.

The BER relation for MQAM (M-ary quadrature amplitude modulation) using the signal-space concept is extracted as [8]:

$$P_{e,MQAM} \cong \frac{4}{\log_2 M}\left(1-\frac{1}{\sqrt{M}}\right)\sum_{i=1}^{\sqrt{M}/2} Q\left((2i-1)\sqrt{\frac{3E_b \log_2 M}{(M-1)N_o}}\right) \tag{9.3}$$

It is shown that, using only the first term in (9.3), the BER can be closely approximated as [8]:

$$P_{e,MQAM} \cong \frac{4}{\log_2 M}\left(1-\frac{1}{\sqrt{M}}\right)Q\left(\sqrt{\frac{3E_b \log_2 M}{(M-1)N_o}}\right) \tag{9.4}$$

It is a straightforward task to extract the BER of MQAM due to a sample function of θ_n using same procedure as in [8], [9]:

$$p_{pn}(M,\theta_n) = \frac{4(\sqrt{M}-1)}{M\log_2(M)} \sum_{i=\frac{-\sqrt{M}}{2}}^{\frac{\sqrt{M}}{2}-1} Q\left(\left(1-(2i+1)\sin\theta_n\right)\sqrt{\frac{3\gamma_s}{M-1}}\right) \tag{9.5}$$

where γ_s denotes the received signal-to-noise ratio (SNR) (i.e. $\gamma_s = received\ signal\ power / \sigma_w^2$) and M is the constellation size. Hence, the

BER can be approximated as $p_b(\theta_n) \cong \frac{SER(\theta_n)}{\log_2(M)}$. This relation provides the same results as in [8], [9], if $\theta_n = 0$. The average BER is obtained by taking the expected value of (9.5) with respect to the probability density function (pdf) of θ_n ; therefore:

$$P_e(M) = \int_{-\infty}^{\infty} p_{pn}(M, \theta_n) f_{\Theta_n}(\theta_n) d_{\theta_n} . \tag{9.6}$$

SISO Case Study

In a SISO scenario, one transmitter and one receiver are connected in an AWGN channel. The analytic, simulation and measurement results of the SISO system over the AWGN channel using a very low phase noise oscillator are presented in Figure 9.1. The measurement setup is discussed in the appendix. As can be seen, the simulation agrees very well with the analytic results. However, there is a gap of about 1 dB between the analytical and measurement results. This is due to implementation loss and the phase noiseless assumption of the signal generators that operate as LOs. Nevertheless, there is good agreement between analytical and measurement results. Figure 9.2 shows the results of the SISO system over the AWGN channel with phase noise. As shown, the measurement and analytical results are well matched.

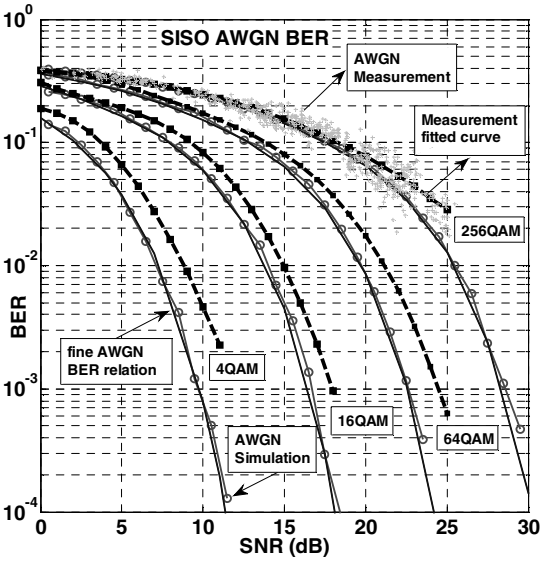

Fig. 9.1 BER of AWGN SISO without phase noise

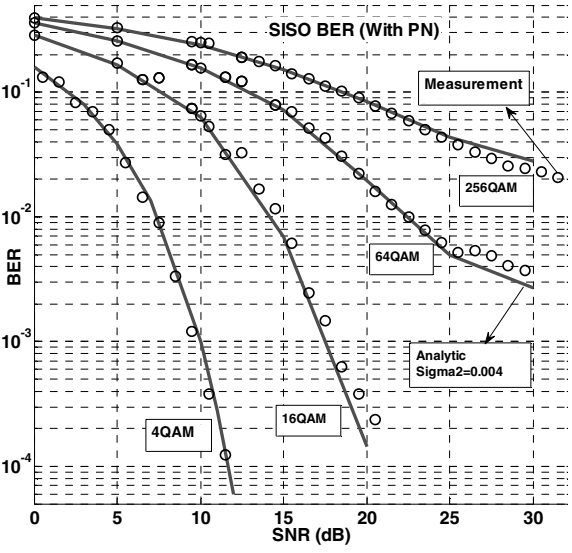

Fig. 9.2 BER of AWGN SISO with phase noise (PN)

9.1.2 Impact of Phase Noise on MIMO Systems

A flat-fading MIMO channel with N_T transmitting antennas and N_R receiving antennas is considered. Assuming perfect synchronization, the input-output relationship is given by:

$$\mathrm{y}=\mathrm{Hx}+\mathrm{w} \tag{9.7}$$

where y is an $N_R \times 1$ vector of the received signal, H denotes the $N_R \times N_T$ channel matrix, x is an $N_T \times 1$ vector of transmitted symbols, and w is an $N_R \times 1$ additive white Gaussian noise vector. The channel coefficients $\left\{h_{\mu\upsilon}\right\}_{\mu=1,\upsilon=1}^{N_R,N_T}$ are statistically i.i.d. complex-valued Gaussian random variables with a variance of 1. Components of the noise vector have the same distribution with a variance of N_0.

If singular value decomposition (SVD) is applied to H, it can be expressed as

$$\mathrm{H}=\mathrm{UDV}^H \tag{9.8}$$

where $(.)^H$ denotes the conjugate transpose; D is an $N_R \times N_T$ matrix with singular values of H, and $\left\{\sqrt{\lambda_i}\right\}_{i=1}^{m}$ and $m \overset{\Delta}{=} \min(N_t, N_r)$, are its main diagonal elements;

U and V are $N_R \times N_R$ and $N_T \times N_T$ unitary matrices with left and right singular vectors of H as their columns, respectively. Substituting (9.8) into (9.7) we have:

$$y' = Dx' + w' \tag{9.9}$$

where:

$$y' \overset{\Delta}{=} U^H y \,,\; x' \overset{\Delta}{=} V^H x \,,\; w' \overset{\Delta}{=} U^H w \tag{9.10}$$

Since $\boldsymbol{U}$ and $\boldsymbol{V}$ are unitary matrices, the powers of x and x' are the same, as well y and y', w and w'. The equivalent model of the system is depicted in Figure 9.3, which shows that the MIMO channel is converted into m parallel SISO subchannels by SVD.

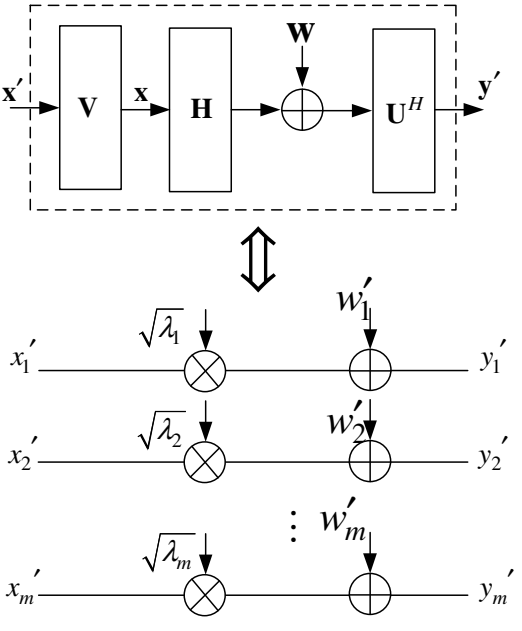

Fig. 9.3 MIMO system and equivalent model

Due to the randomness of the entries of H, the subchannel power gain (λ) is a random process. The marginal pdf of the unordered eigenvalues is [10]

$$Pdf_{\lambda_1}(\lambda_1) = \frac{1}{m}\sum_{k=0}^{m-1} \frac{k!}{(k+d)!}\left[L_k^d(\lambda_1)\right]^2 \lambda_1^d e^{-\lambda_1} \tag{9.11}$$

where $L_k^d(\lambda_1)$ is the associated Laguerre polynomial of order k, i.e.:

$$L_k^d(\lambda_1) = \sum_{l=0}^{k} (-1)^l \frac{(k+d)!}{(k-l)!(d+l)!l!} \lambda_1^l \tag{9.12}$$

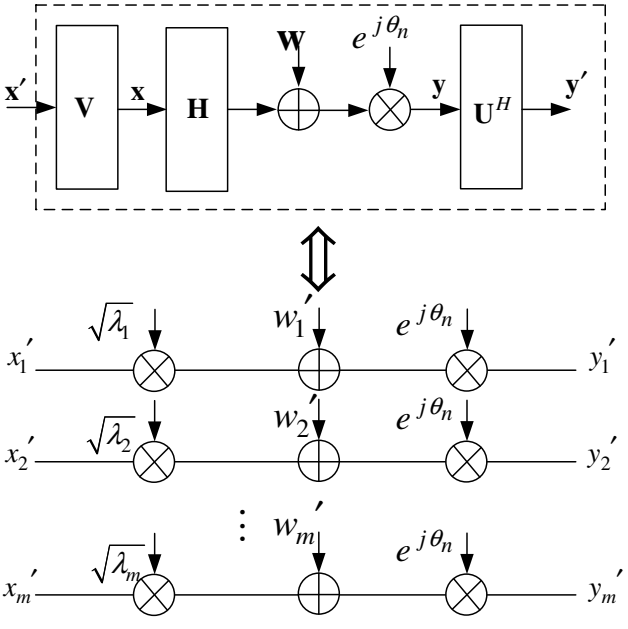

Fig. 9.4 MIMO system and equivalent model with phase noise

The MIMO system model with phase noise is presented in Figure 9.4. The input-output relationship is given by:

$$\mathbf{y}=\mathbf{\Theta}\mathbf{H}\mathbf{x}+\mathbf{\Theta}\mathbf{w} \tag{9.13}$$

where $\mathbf{\Theta}$ is an $N_R \times N_R$ matrix of phase noise and is defined as follows:

$$\Theta = \begin{pmatrix} e^{j\theta_1} & & 0 \\ & \ddots & \\ 0 & & e^{j\theta_1} \end{pmatrix}_{N_R \times N_R} \tag{9.14}$$

Equation (9.13) can be rewritten as:

$$y' = \mathrm{U}^{\mathrm{H}}\boldsymbol{\Theta}\mathrm{H}Vx' + \mathrm{U}^{\mathrm{H}}\boldsymbol{\Theta}w \tag{9.15}$$

Since the $\boldsymbol{\Theta}$ is diagonal, (9.13) can be written as (9.15); and, since the $\boldsymbol{\Theta}$ is diagonal and its entries have unit norm and random phase, the entries of $\boldsymbol{\Theta}w'$ are complex Gaussian random variables with a zero mean and a variance of N_0. It is easy to see that the received signal can be again converted into m parallel SISO subchannels by SVD. The difference from the previous situation is that each subchannel is affected by similar phase noise.

$$y' = \boldsymbol{\Theta}\mathrm{U}^{\mathrm{H}}\mathrm{H}Vx' + \boldsymbol{\Theta}w' = \boldsymbol{\Theta}Dx' + \boldsymbol{\Theta}w' \tag{9.16}$$

MIMO Case Study

The results of the MIMO system with adaptive modulation using $N_T = N_R = 4$ are presented. The Rayleigh fading channel is used in the channel simulator. Moreover, we used zero forcing receivers for MIMO detection. Figure 9.5 shows the results. As shown, there is good agreement between the analytic and measurement results.

9.1.3 Adaptive Modulation MIMO System

In the adaptive modulation scheme, the channel is estimated in the receiver and fed back to the transmitter. The transmitter adapts the transmitting signal, considering the feedback information, in order to maximize the spectral efficiency. We assume that the feedback path does not introduce any errors and delay. The availability of channel information at the transmitter allows it to adapt its transmission power and rate relative to the channel variation [9].

A variable-rate variable-power (VRVP) adaptation scheme is considered here. According to the above decomposition, the adaptive modulation MIMO problem can be considered as an adaptive modulation SISO problem using the unordered eigenvalue distribution [12]. Hence, the following problem should be solved by maximizing the average spectral efficiency (ASE) [13]:

$$\begin{aligned} &\underset{P_1,k_1}{\text{maximize}} \quad ASE = m\varepsilon_{\lambda_1}\left[k_1(\lambda_1)\right] \\ &\text{subject to } \varepsilon_{\lambda_1}\left[P_1(\lambda_1)\right] = P/m \\ &BER_1(\lambda_1) = BER_{tgt} \end{aligned} \tag{9.17}$$

where λ_1 is the first unordered subchannel power gain, and P_1, k_1 and BER_1 are the power, rate and instantaneous BER in the first unordered subchannel, respectively. We use only square MQAMs; therefore, the available rates are:

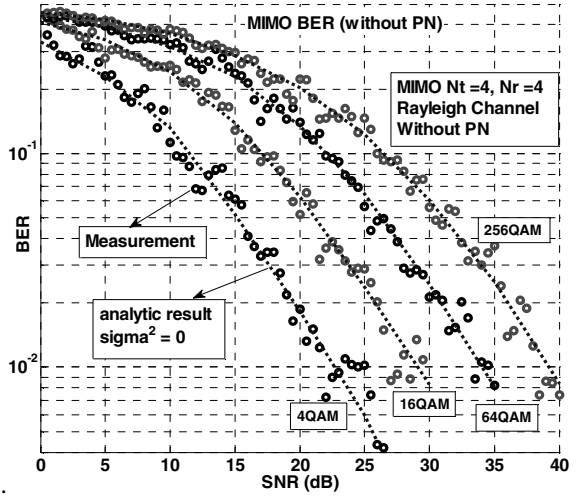

(a)

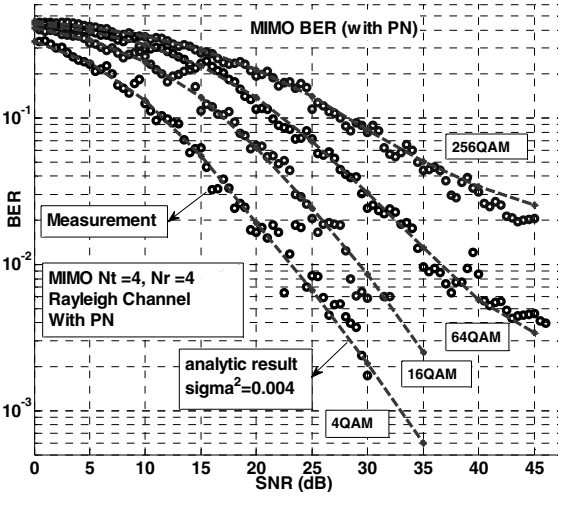

(b)

Fig. 9.5 Rayleigh MIMO: (a) without phase noise, (b) with phase noise

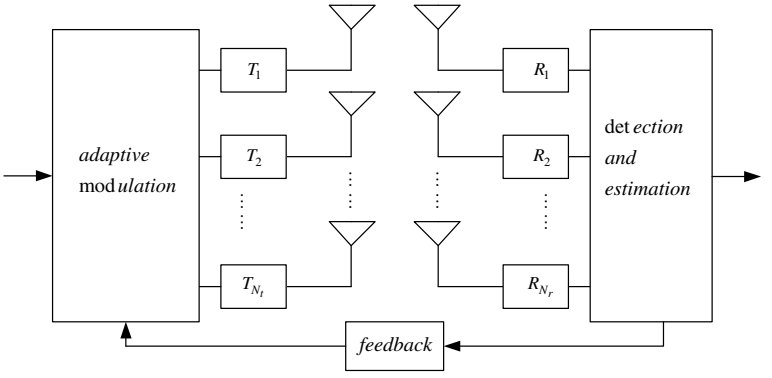

Fig. 9.6 An adaptive modulation MIMO structure

$$\begin{aligned} &k_1(\lambda_1) \in \{r_0, r_1, \ldots, r_N\} \\ &r_i = 2i \quad i = 0,1,\ldots,N \end{aligned} \tag{9.18}$$

The solution to the problem in (9.17) has been given in [3]. Therefore, the optimal power and rate policy is:

$$\begin{cases} k_1(\lambda_1) = r_i, & \upsilon_i \le \lambda_1 < \upsilon_{i+1} \\ P_1(\lambda_1) = \dfrac{M_i - 1}{\lambda_1} \dfrac{\sigma_w^2}{K}, & \upsilon_i \le \lambda_1 < \upsilon_{i+1} \end{cases} \tag{9.19}$$

where $M_i = 2^{r_i}$, $K = \dfrac{-1.5}{\ln(5BER_{tgt})}$ and υ_i denotes the power gain boundary and equals to

$$\upsilon_i = \frac{M_i - M_{i-1}}{r_i - r_{i-1}} \frac{\mu}{K} \tag{9.20}$$

where $\mu > 0$ and is the Lagrangian multiplier that is determined from the average power constraint equation:

$$\sum_{i=1}^{N} \frac{M_i - 1}{K} \left[\int_{\upsilon_i}^{\infty} \frac{Pdf_{\lambda_1}(\lambda_1)}{\lambda_1} d\lambda_1 - \int_{\upsilon_{i+1}}^{\infty} \frac{Pdf_{\lambda_1}(\lambda_1)}{\lambda_1} d\lambda_1 \right] = \frac{P}{m\sigma_w^2} \tag{9.21}$$

After obtaining μ, the average spectral efficiency can be achieved from:

$$R = m \sum_{i=1}^{N} r_i \left[\int_{\upsilon_i}^{\infty} Pdf_{\lambda_1}(\lambda_1) d\lambda_1 - \int_{\upsilon_{i+1}}^{\infty} Pdf_{\lambda_1}(\lambda_1) d\lambda_1 \right] \tag{9.22}$$

9.1.4 BER of Adaptive Modulation MIMO System with Phase Noise

The average BER of the system can be expressed as:

$$Average\ BER = \frac{\sum_{j=1}^{N} P_e(M_j) \times \log_2(M_j) P(\upsilon_j \le \lambda_1 < \upsilon_{j+1})}{\sum_{j=1}^{N} \log_2(M_j) P(\upsilon_j \le \lambda_1 < \upsilon_{j+1})} \tag{9.23}$$

where $P_e(M_j)$ is the BER corresponding to M_j, and $P(\upsilon_j \le \lambda_1 < \upsilon_{j+1})$ is the probability that λ_1 falls in the *j*th region, so that:

$$p(\upsilon_j \le \lambda_1 < \upsilon_{j+1}) = \int_{\upsilon_j}^{\upsilon_{j+1}} Pdf_{\lambda_1}(\lambda_1) d\lambda_1 \tag{9.24}$$

From (9.17), the received signal power (P_{rec}) due to adaptive modulation can be expressed as:

$$P_{rec} = \lambda_1 P_1(\lambda_1) = \frac{-2\ln(5BER_{tgt})\sigma_w^2}{3}\left(M_i - 1\right) \tag{9.25}$$

From (9.5) and (9.25), for a sample function of θ_n, $P_e(M_j)$ can be written:

$$p_{pn}(M_j, \theta_n) = \frac{4(\sqrt{M_j} - 1)}{M_j \log_2(M_j)} \sum_{i=\frac{-\sqrt{M_j}}{2}}^{\frac{\sqrt{M_j}}{2}-1} Q\left(\left(1 - (2i+1)\sin\theta_n\right)\sqrt{-2\ln(5BER_{tgt})}\right) \tag{9.26}$$

The BER of the system for a constellation size of M_j is obtained by taking the expected value of (9.26) with respect to θ_n , so that:

$$P_e(M_j) = \int_{-\infty}^{\infty} \frac{1}{\sqrt{2\pi}\sigma_{\theta_n}} p_{pn}(M_j, \theta_n) e^{\frac{-\theta_n^2}{2\sigma_{\theta_n}^2}} d_{\theta_n} \tag{9.27}$$

Therefore, the total BER of the adaptive modulation MIMO system under the impact of phase noise can be expressed in a closed form as:

$$BER_{PN} = \frac{\sum_{j=1}^{N}\left[P_e(M_j) \times \log_2(M_j) \times \int_{\upsilon_j}^{\upsilon_{j+1}} Pdf_{\lambda_1}(\lambda_1) d\lambda_1 \right]}{\sum_{j=1}^{N}\left[\log_2(M_j) \times \int_{\upsilon_j}^{\upsilon_{j+1}} Pdf_{\lambda_1}(\lambda_1) d\lambda_1 \right]} \tag{9.28}$$

Case Study: Adaptive Modulation MIMO

The performance of the adaptive modulation MIMO system under the impact of phase noise is presented in this section. The measurement results of the adaptive modulation MIMO system are presented for a set of average SNRs, $N_T = N_R = 4$ and $k_1(\lambda_1) \in \{0,2,4,6,8\}$. The Rayleigh fading channel is used in the channel simulator. A BER_{tgt} of 10^{-2} is selected for our measurements. Perfect channel state information (P-CSI) is assumed at both the transmitter and receiver [14], [15]. However, the phase noise affects the channel estimation. The channel is estimated in the receiver and fed back to the transmitter. To determine the training sequence length, we use the available algorithm [16]. Due to P-CSI, the total average spectral efficiency, which is only related to channel model and average SNR, is the same as the case without phase noise. This is validated in Figure 9.7 using simulation and measurement results.

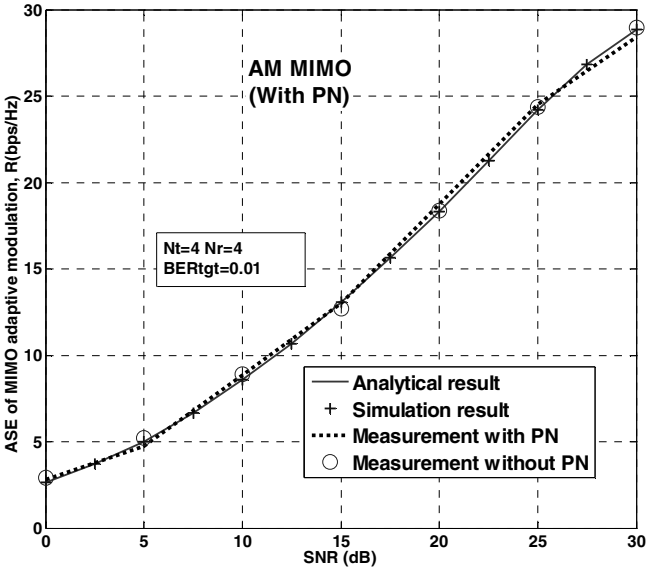

Fig. 9.7 ASE of adaptive modulation MIMO system under impact of phase noise ($BER_{tgt} = 10^{-2}$, $SNR = \frac{P}{\sigma_w^2}$)

In Figure 9.8-a, the measurement results of an adaptive modulation MIMO system in a Rayleigh channel without phase noise are depicted. As shown, the measurement results are close to the analytical results.The measurement results of an adaptive modulation MIMO system over a Rayleigh channel with phase noise are shown in Figure 9.8-b. This figure shows an unusual behavior, where by increasing the average SNR, the BER is more degraded. This is due to the use of higher constellation sizes in larger SNRs by the adaptive modulator. The higher constellation

sizes are more sensitive to the phase noise. Hence, the total impact of higher constellation sizes and greater sensitivity to phase noise results in BER degradation. As can be seen in this figure, there is good agreement between the measurement and analytical results.

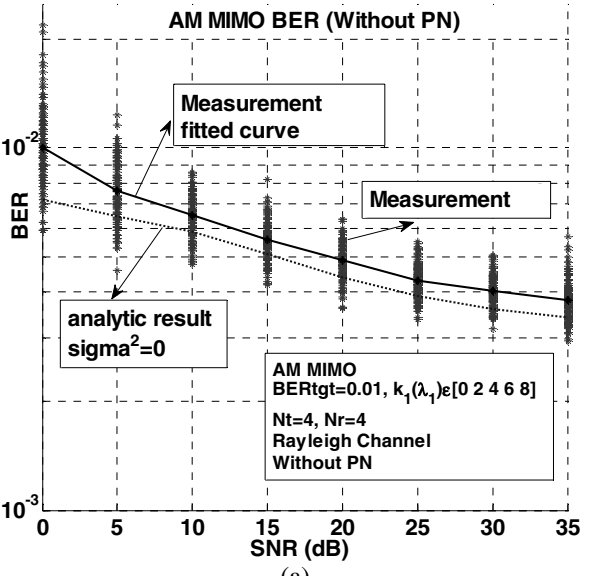

(a)

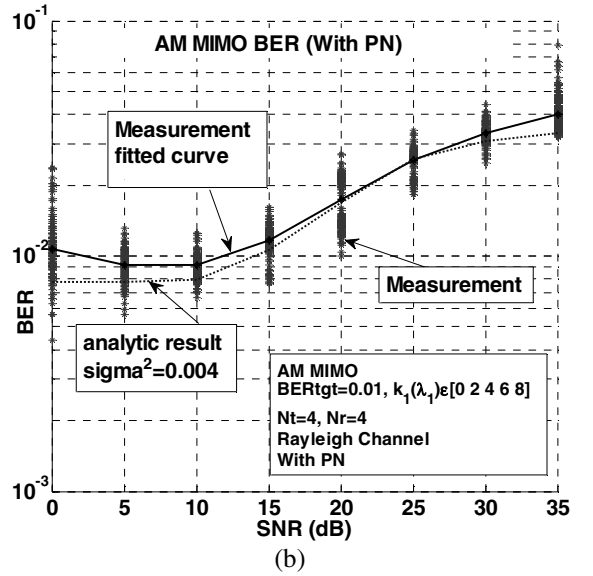

(b)

Fig. 9.8 BER of an adaptive MIMO system: (a) without phase noise, (b) with phase noise

The average spectral efficiency (ASE) of an adaptive modulation (AM) MIMO system for six various antennas configurations are shown in Figure 9.9. The results are obtained with $BER_{tgt} = 10^{-3}$ and $k_1(\lambda_1) \in \{0,2,4,6,8,10\}$,and agree with the available literature [12].

The average BER rate versus the variance of phase noise, $\sigma_{\theta_n}^2$, for different SNR values are shown in Figure 9.10. The average BERs are presented for a BER_{tgt} equal to .01 and .001. As expected, by increasing the phase noise power, the BER is more degraded.

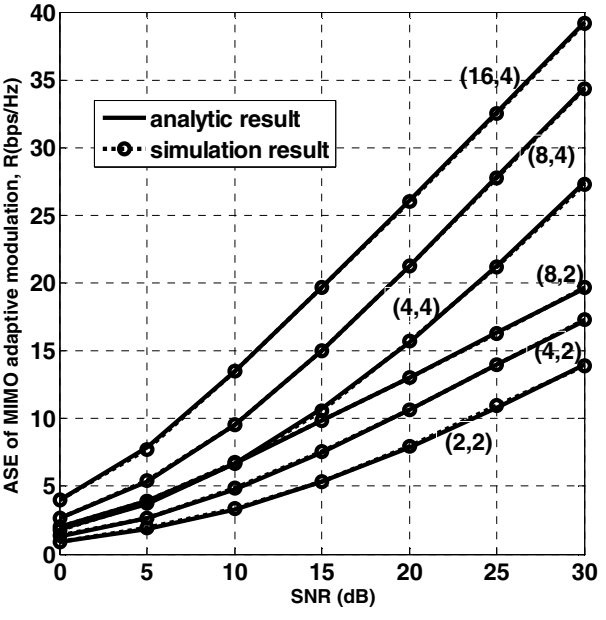

Fig. 9.9 ASE of an AM MIMO system ($BER_{tgt} = 10^{-3}$, $k_1(\lambda_1) \in \{0,2,4,6,8,10\}$, $SNR = \frac{P}{\sigma_n^2}$)

9.2 DC Offset in MIMO Transceivers

The DC offset is the other impairment that reduces the performance of MIMO transceivers. In this section, the DC offset impairment is investigated. The complete removal of the DC offset in the receiver can be very difficult; therefore, the baseband compensations are usually required [19].

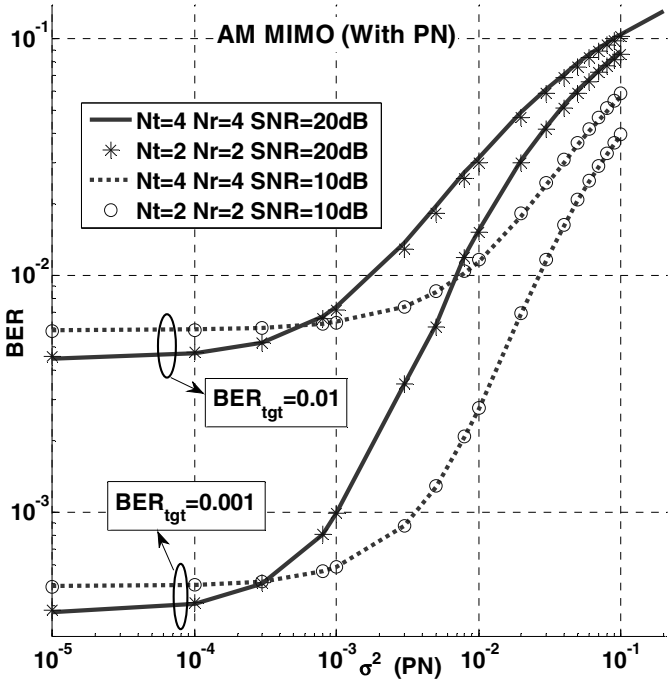

Fig. 9.10 Average BER of an AM MIMO system versus $\sigma_{\theta_n}^2$ (analytic results)

9.2.1 DC Offset

The DC offset sources can be broken down into static DC error and dynamic DC [20]. Static DC errors are generally caused by self-mixing of an LO within the receiver itself. On the other hand, dynamic DC errors are caused by time-varying effects within the receiver environment. Some examples of the dynamic DC offset errors are [21], [22]:

- Reflections of the receiver LO, which is radiated from the receiver antenna and are picked up by receiver and down-converted to DC.
- Rapid changes in signal strength (such as those caused by fading), which are not tracked quickly enough by the receiver automatic gain control (AGC). The receiver is overloaded for a short period of time, and second-order nonlinearity causes the DC offset.

DC offset degrades the BER of the receiver. It may also saturate the baseband analog-to-digital converters (ADCs), which dramatically reduces their dynamic range. Therefore, the DC offset must be removed by means of a calibration method.

Sometimes a capacitive coupling can be used, although it removes some of the wanted signal energy. When the signal has significant energy at or close to DC, capacitive coupling is not an option; however, it is possible to perform DC calibration, which is done by injecting an appropriate DC level to cancel the DC offset.

The measurement process is typically performed in the digital domain by long-term averaging. The calculated DC offset is subtracted from the received signal (typically in the analog domain). DC calibration has a disadvantage in that it is not capable of completely compensating for dynamic DC offsets, whereas static DC offsets can just be removed. In the remainder of this section, wherever DC offset mentioned, it means the uncompensated part of the DC offset. Since the nature of a dynamic DC offset is random and is best modeled by a zero-mean complex Gaussian distributed random variable [23], we assume the same model for the uncompensated part.

9.2.2 BER OF MQAM Modulation under Impact of DC Offset

In this section, a closed form expression for the MQAM BER under the impact of DC offset is extracted. The relation between the input and output of a digital communication system can be written as:

$$s' = s + c + w \tag{9.29}$$

where $s = s_I + js_Q$ is the transmitted signal, $c = c_I + jc_Q$ is the DC offset, s' is the received signal, and w is the AWGN.

It is assumed that static DC offsets have been removed entirely and that the remaining DC offset is modeled as a zero-mean, complex Gaussian distributed random variable. It is considered that the channel varies very slowly, as well as the DC offset; and, the channel is constant in the transmission interval of a frame. (Since the sources of dynamic DC offset are related to the time-varying effects within the receiver environment, the same flat model as the channel model is acceptable for DC offset.)

The constellation diagram of a square QAM signal is depicted in Figure 9.9. This figure shows the s and s' points with Gray-encoded bit mapping. If we use the method of signal-space concepts or the method of [25], the BER for a specific realization of c is:

$$P_b^{MQAM}(d,c) \cong \frac{\left(1-{}^{1}\!/\!_{\sqrt{M}}\right)}{\log_2 M} \times \sum_{i=1}^{\sqrt{M}/2} \left\{ Q\left(\frac{(2i-1)d + c_I}{{}^{\sigma_w}\!/\!_{\sqrt{2}}} \right) + Q\left(\frac{(2i-1)d + c_Q}{{}^{\sigma_w}\!/\!_{\sqrt{2}}} \right) + Q\left(\frac{(2i-1)d - c_I}{{}^{\sigma_w}\!/\!_{\sqrt{2}}} \right) + Q\left(\frac{(2i-1)d - c_Q}{{}^{\sigma_w}\!/\!_{\sqrt{2}}} \right) \right\} \tag{9.30}$$

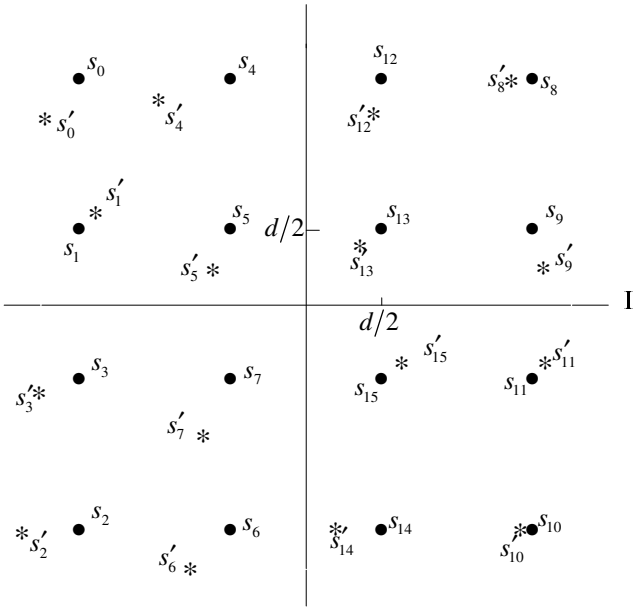

Fig. 9.9 The constellation diagram of a 16-QAM signal

where d is the Euclidean distance of two adjacent points. The Q function is very low for a large argument, so we can approximate relation (9.30) to:

$$P_b^{MQAM}(d,c) \cong \frac{\left(1-1/\sqrt{M}\right)}{\log_2 M} \times \left\{ Q\left(\frac{d+c_I}{\sigma_w/\sqrt{2}}\right) + Q\left(\frac{d+c_Q}{\sigma_w/\sqrt{2}}\right) + Q\left(\frac{d-c_I}{\sigma_w/\sqrt{2}}\right) + Q\left(\frac{d-c_Q}{\sigma_w/\sqrt{2}}\right) \right\} \tag{9.31}$$

It is known that c_I and c_Q are Gaussian with a zero-mean value and a variance of $\sigma_c^2/2$ and that:

$$\frac{d}{\sigma_w} = \sqrt{\frac{3\gamma_s}{2(M-1)}},$$

where $\gamma_s = \frac{\textit{received signal power}}{\sigma_w^2}$ is the received symbol SNR, and σ_w^2 is the AWGN variance.

After some calculations, the MQAM BER under the impact of a DC offset is approximated as:

$$P_{DC}(M) = P_b^{MQAM}(\gamma_s) \cong \frac{4\left(1-{}^{1}/_{\sqrt{M}}\right)}{\sqrt{\frac{2\pi P}{m\sigma_w^2 SDCR}}\log_2 M} \times \int_0^{\infty}\left[Q\left(\sqrt{\frac{3\gamma_s}{M-1}}+\beta\right)+Q\left(\sqrt{\frac{3\gamma_s}{M-1}}-\beta\right)\right] e^{\frac{-m\sigma_w^2\beta^2}{{}^{2P}/_{SDCR}}}\, d\beta \tag{9.32}$$

where $SDCR \overset{\Delta}{=} {}^{P}/_{m\sigma_c^2}$ (signal-to-DC ratio).

9.2.3 MIMO System Model

Each receiving path is impaired by a DC offset, which causes BER degradation in comparison with the ideal case. The input signal, x ($N_t \times 1$), and the output signal, y ($N_r \times 1$), are related by:

$$\mathrm{y} = \mathrm{H}\mathrm{x} + \mathrm{w} + \mathrm{c} \tag{9.33}$$

where w ($N_r \times 1$) is the AWGN and its entries are independent and $w_i \sim \mathcal{CN}(0, \sigma_w^2)$; and, c ($N_r \times 1$) is the DC offset.

The following definitions are supposed:

$$m \overset{\Delta}{=} \min(N_t, N_r), \quad n \overset{\Delta}{=} \max(N_t, N_r), \quad d \overset{\Delta}{=} n - m \tag{9.34}$$

If singular value decomposition (SVD) is applied to H, (9.33) is converted to:

$$\mathrm{y}' = \mathrm{D}\mathrm{x}' + \mathrm{w}' + \mathrm{c}' \tag{9.35}$$

where:

$$\mathrm{y}' \overset{\Delta}{=} \mathrm{U}^H\mathrm{y}, \ \mathrm{x}' \overset{\Delta}{=} \mathrm{V}^H\mathrm{x}, \ \mathrm{w}' \overset{\Delta}{=} \mathrm{U}^H\mathrm{w}, \ \mathrm{c}' \overset{\Delta}{=} \mathrm{U}^H\mathrm{c} \tag{9.36}$$

and U, V and D are the decomposing elements of H, which means $\mathrm{H}=\mathrm{U}\mathrm{D}\mathrm{V}^H$.

U and V are unitary matrices, so the powers of x and x', y and y', w and w', c and c' are the same, respectively. D is a diagonal matrix with the singular values of H, with $\left\{\sqrt{\lambda_i}\right\}_{i=1}^{m}$ as its main diagonal elements. As discussed in the previous section, a MIMO channel by SVD is converted into m parallel SISO subchannels.

9.2.4 BER of Adaptive Modulation MIMO under the Impact of DC Offset

In this section we investigate the impact of DC offset on adaptive modulation in MIMO systems. It is assumed that all subchannels have been impaired by the DC offset with identical variances, so the total bit error probability is equal to the average BER in each subchannel. The average BER in each subchannel can be expressed as:

$$Average\ BER = \frac{\sum_{j=1}^{N} P_{DC}(M_j) \times \log_2(M_j) P(\upsilon_j \le \lambda_1 < \upsilon_{j+1})}{\sum_{j=1}^{N} \log_2(M_j) P(\upsilon_j \le \lambda_1 < \upsilon_{j+1})} \tag{9.37}$$

where $P_{DC}(M_j)$ is the BER that corresponds to M_j, and $P(\upsilon_j \le \lambda_1 < \upsilon_{j+1})$ is the probability that λ_1 falls in the jth region, so that:

$$p(\upsilon_j \le \lambda_1 < \upsilon_{j+1}) = \int_{\upsilon_j}^{\upsilon_{j+1}} P df_{\lambda_1}(\lambda_1) d\lambda_1 \tag{9.38}$$

The adaptation scheme is

$$received\ signal\ power = \lambda_1 P_1(\lambda_1) = \frac{-2\ln(5BER_{tgt})\sigma_w^2}{3}(M_i - 1) \tag{9.39}$$

From (9.32), the $P_{DC}(M_j)$, under the impact of DC offset in the adaptation scheme, can be written as:

$$P_{DC}(M_j) \cong \frac{4\left(1 - 1/\sqrt{M_j}\right)}{\sqrt{\frac{2\pi P}{m\sigma_w^2 SDCR}} \log_2 M_j} \times \int_0^{\infty} \left[Q\left(\sqrt{-2\ln(5BER_{tgt})} + \beta\right) + Q\left(\sqrt{-2\ln(5BER_{tgt})} - \beta\right) \right] e^{\frac{-m\sigma_w^2\beta^2}{2P/SDCR}} d\beta \tag{9.40}$$

Therefore, the total BER of MIMO adaptive modulation under the impact of DC offset can be achieved as:

$$BER_T = Average\ BER \tag{9.41}$$

where BER_T is the total BER of the adaptive MIMO system, including the effect of the DC offset.

9.2.5 BER Upper Bound of Adaptive Modulation under the Impact of DC Offset

In [26], the following upper bound relation is used for computation of the AM power gain boundaries:

$$BER \le 0.2\exp\left(\frac{-1.5\gamma_s}{M-1}\right) \tag{9.42}$$

where γ_s is the symbol SNR.

To improve the DC-affected AM system, adaptation should be done with respect to the DC offset, because a DC offset degrades the AM MIMO BER, allowing it to become greater than BER_{tgt}. If we change the mechanism of adaptation by considering DC offset, we may have a BER better than BER_{tgt}.

In order to obtain the optimal power and rate adaptation for different modulation schemes, we need an expression for each modulation technique's BER in AWGN that is easily inverted, with respect to rate and power.

Unfortunately, the approximated DC affected BERis neither easily invertible nor easily differentiable in its argument, but these properties are needed for adaptive modulation design. Therefore, we now introduce a new tight BER approximation for MQAM affected by DC offset in AWGN, which can be easily differentiated and inverted. The following upper bound for (9.32) is an acceptable approximation for optimal adaptation:

$$P_{DC}(M) \le 0.2\exp\left(\frac{-1.5\gamma_s}{(M-1)\left(1+\dfrac{P}{m\sigma_w^2 SDCR}\right)}\right) \tag{9.43}$$

As can be seen, the variance of noise (σ_w^2) has been added to the variance of the DC offset (σ_c^2); and, an upper bound relation for the BER in the presence of DC offset has been calculated from (9.42) (replacing σ_w^2 by $\sigma_w^2+\sigma_c^2$). It is a logical approximation due to the nature of the dynamic DC offset, as explained in Section 4. The accuracy of this approximation has been verified by simulation and is shown in Figure 9.12. Based on this upper bound, a new adaptation mechanism is used:

$$\begin{cases} k_1(\lambda_1) = r_i, & \upsilon_i' \le \lambda_1 < \upsilon_{i+1}' \\ P_1(\lambda_1) = \dfrac{M_i - 1}{\lambda_1}\dfrac{\sigma_w^2}{K}\left(1+\dfrac{P}{m\sigma_w^2 SDCR}\right), & \upsilon_i' \le \lambda_1 < \upsilon_{i+1}' \end{cases} \tag{9.44}$$

where

$$\upsilon_i' = \frac{M_i - M_{i-1}}{r_i - r_{i-1}} \frac{\mu}{K} \left(1 + \frac{P}{m\sigma_w^2 \, SDCR} \right) \tag{9.45}$$

and μ is calculated from:

$$\sum_{i=1}^{N} \frac{M_i - 1}{K} \left[\int_{\upsilon_i'}^{\infty} \frac{P df_{\lambda_1}(\lambda_1)}{\lambda_1} d\lambda_1 - \int_{\upsilon_{i+1}'}^{\infty} \frac{P df_{\lambda_1}(\lambda_1)}{\lambda_1} d\lambda_1 \right] = \frac{P}{m\sigma_w^2 \left(1 + \frac{P}{m\sigma_w^2 \, SDCR} \right)} \tag{9.46}$$

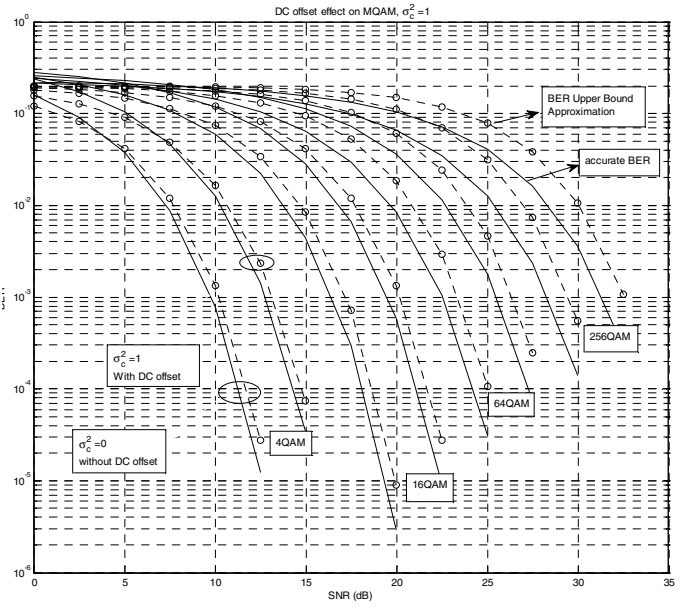

Fig. 9.12 The accurate and approximate BER under the impact of DC offset

In this case, the BER is calculated as:

$$P_{DC}(M_j) \cong \frac{4\left(1-1/\sqrt{M_j}\right)}{\sqrt{\frac{2\pi P}{m\sigma_w^2 SDCR}\log_2 M_j}} \times \int_0^{\infty}\left[Q\left(\sqrt{-2\ln(5BER_{tgt})\left(1+\frac{P}{m\sigma_w^2 SDCR}\right)}+\beta\right) + Q\left(\sqrt{-2\ln(5BER_{tgt})\left(1+\frac{P}{m\sigma_w^2 SDCR}\right)}-\beta\right)\right] e^{\frac{-m\sigma_w^2\beta^2}{2P/SDCR}}\, d\beta \tag{9.47}$$

The ASE is calculated from (9.22) with v_i' instead of v_i.

9.2.6 Throughput Analysis

The throughput is defined as the ratio of the average number of bits in packets that are successfully transmitted in any given time interval, divided by the number of attempted transmissions in that interval [29]. It is a key measure of quality of service (QoS) for wireless data transmission systems. The transmitter constructs the packet and transmits it through the air. The receiver processes the received packet. Upon detecting the packet, the receiver sends an acknowledgment, either positive or negative, back to the transmitter. For ease of analysis we assume this feedback packet goes through a separate control channel and arrives at the transmitter instantaneously and without error. If the receiver detects any error and issues a negative acknowledgement, the transmitter uses a selective repeat protocol to resend the packet. It repeats the process until the packet is successfully delivered.

We define the throughput of a system as the number of payload bits received correctly per second:

$$T = \frac{L-C}{L} R_b P_{sp} \tag{9.48}$$

where T is the throughput, L is the packet length, C is the non-information bits in a packet, R_b is the bit rate, and P_{sp} is the packet success probability. It is assumed that $L >> C$, so $\frac{L-C}{L}$ is ignored; therefore, $T = R_b P_{sp}$.

R_b is the bit rate, so it is equal to $R_b = R_s r_{i_1} + R_s r_{i_2} + \ldots + R_s r_{i_m} = R_s(r_{i_1} + \ldots + r_{i_m})$, where r_{i_1} is the number of bits per each symbol in the first subchannel, r_{i_2} is the number of bits per each symbol in the second subchannel … to r_{i_m}, which is the number of bits per each symbol in the last subchannel.

R_s is the symbol rate in each subchannel. Each packet contains N_s symbols in the first subchannel, N_s symbols in the second subchannel ... to N_s symbols in the last subchannel. The BER in the first subchannel is $P_b(r_{i_1})$ and $P_b(r_{i_2})$ in the second subchannel ... to $P_b(r_{i_m})$ in the last subchannel. The probability that all the bits are transmitted successfully in the first subchannel is $\left(1-P_b(r_{i_1})\right)^{N_s r_{i_1}}$ and … to $\left(1-P_b(r_{i_1})\right)^{N_s r_{i_m}}$, which is the probability that all the bits are transmitted successfully in the last subchannel .

Since any bit error in the packet results in a loss of the packet, the P_{sp} in our VRVP AM system is calculated as:

$$P_{sp} = \left(1-P_b(r_{i_1})\right)^{N_s r_{i_1}} \ldots\ldots \left(1-P_b(r_{i_m})\right)^{N_s r_{i_m}} \tag{9.49}$$

where N_s is the number of symbols in each subchannel, r_{i_j}, $j=1,...,m$ is the number of bits per each symbol of the *j*th subchannel, and $P_b(r_{i_j})$ is the error probability of a bit. Now the throughput can be calculated as:

$$\begin{aligned} T(r_{i_1},\ldots,r_{i_m}) &= R_s(r_{i_1}+\ldots+r_{i_m}) \\ &\times\left(1-P_b(r_{i_1})\right)^{N_s r_{i_1}} \ldots\ldots \left(1-P_b(r_{i_m})\right)^{N_s r_{i_m}} \end{aligned} \tag{9.50}$$

where R_s is the symbol rate of the system and is the same for all subchannels. Finally, the average throughput is obtained as:

$$\begin{aligned} AT = \sum_{i_1=1}^{N}\ldots\sum_{i_m=1}^{N} T(r_{i_1},\ldots,r_{i_m})\times \\ p(\upsilon_{i_1}\le\lambda_1<\upsilon_{i_1+1},\ldots,\upsilon_{i_m}\le\lambda_m<\upsilon_{i_m+1}) \end{aligned} \tag{9.51}$$

where $p(\upsilon_{i_1}\le\lambda_1<\upsilon_{i_1+1},\ldots,\upsilon_{i_m}\le\lambda_m<\upsilon_{i_m+1})$ is the probability that the constellation size in the first subchannel is $2^{r_{i_1}}$ and in the second subchannel is $2^{r_{i_2}}$ and … to $2^{r_{i_m}}$ in the last subchannel. The probability is calculated using the joint probability density function (pdf) of the unordered eigenvalues [28].

Relation (9.51) is very complicated, so we may approximate it with a simpler relation. For an approximation of (9.51), we may replace the $P_b(r_{i_j})$, $j=1,...,m$, with the average BER (BER_T) by using the average value approximation. On the other hand, the average of $(r_{i_1}+\ldots+r_{i_m})$ is equal to ASE, defined as *R*. Equation (9.51) can be approximated as:

$$AT \approx ASE \times R_s \times \sum_{i_1=1}^{N} \cdots \sum_{i_m=1}^{N} \left(1-P_b(r_{i_1})\right)^{N_s r_{i_1}} \cdots\cdots$$
$$\left(1-P_b(r_{i_m})\right)^{N_s r_{i_m}} \times p(\upsilon_{i_1} \le \lambda_1 < \upsilon_{i_1+1}, \ldots, \upsilon_{i_m} \le \lambda_m < \upsilon_{i_m+1})$$

$$\Rightarrow AT \approx ASE \times R_s \times \sum_{i_1=1}^{N} \cdots \sum_{i_m=1}^{N} \left(1-BER_T\right)^{N_s (r_{i_1}+r_{i_2}+\ldots+r_{i_m})} \times$$
$$p(\upsilon_{i_1} \le \lambda_1 < \upsilon_{i_1+1}, \ldots, \upsilon_{i_m} \le \lambda_m < \upsilon_{i_m+1})$$

$$AT \approx ASE \times R_s \left(1-BER_T\right)^{ASE \times N_s} \tag{9.52}$$

where BER_T is calculated from (9.41).

Equation (9.52) is very simple and easy to detect, but it causes approximation when calculating the average throughput (AT). Accordingly, the BER degradation of AM MIMO systems under the impact of DC offset can be evaluated. The component modulation schemes are uncoded quadrature amplitude modulations (QAMs) with $k_1(\lambda_1) \in \{0, 2, 4, 6, 8, 10\}$.

We set $BER_{tgt} = 10^{-3}$. It is assumed that the channel is known perfectly. At first, the effect of the DC offset on rgw adaptation design is not considered; hence, the ASE remains unchanged (similar to corresponding curves in [28], but later, in the new design of AM, ASE alters). Six transmit-receive antenna configurations are achieved and depicted in Figure 9.13. The simulation results are also depicted in Figure 9.13. For all receiving branches, the DC offset is set to $SDCR = 20\,dB$. The BER_T curve can be achieved from (9.41).

Figure 9.14 shows the BER_T curve for 6 different configurations of transmit-receive antenna in the non-ideal case ($SDCR = 20\,dB$) and the ideal case ($SDCR = Inf$). As can be seen in Figure 9.14, by increasing the number of antennas, the MIMO adaptive modulation BER is less degraded. The SISO system is more degraded in comparison with the MIMO systems. The (2,2) configuration has the worst BER performance, and the (16,4) has the best BER performance among the MIMO systems. This is expected, since according to the definition, σ_c^2 is proportionate to the reverse of m.

The BER of MIMO adaptive modulation under various SDCR values for (2,2) and (4,4) structures is depicted in Figure 9.15. Moreover, Monte Carlo simulation results are shown in Figure 9.15. As expected, by decreasing the $SDCR$, the MIMO adaptive modulation BER is more degraded. Due to the adaptation mechanism in the ideal case, the actual instantaneous BER lies below the BER_{tgt}.

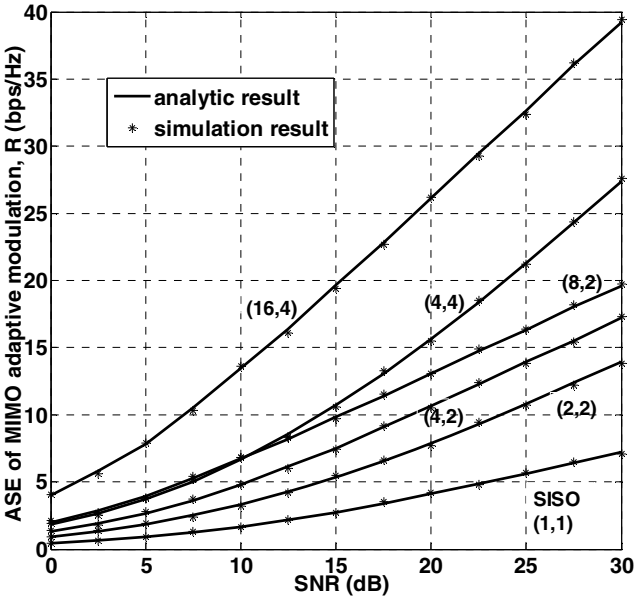

Fig. 9.13 ASE of AM MIMO in 6 various system configurations by supposing $BER_{tgt} = 10^{-3}$, versus $SNR = P/\sigma_w^2$

When the SNR is low or the DC offset is not critical, the actual BER is as good as the ideal case; however, when DC offset gets more severe, the BER becomes greater than BER_{tgt}.

Figures 9.14 and 9.15 also show that the impact of DC offset on the BER is higher for higher SNRs, meaning that the BER is more degraded in the high SNR region. This is because the AM system uses high order component modulations in this region, which are more sensitive to the DC offset. This result can also be seen easily with considering that $\frac{\gamma_s}{(M-1)}$ is constant in VRVP AM systems. It can also be seen that, in low SNRs (low P), the effect of the DC offset is very small, which is also shown in Figures 9.14 and 9.15. The BER of a new design for an AM MIMO system for a (2,2) configuration is depicted in Figure 9.16 ($SDCR = 15\,dB$, $25\,dB$). As shown in this figure, in the new design of AM, the BER remains below $BER_{tgt} = 10^{-3}$.

In Figure 9.17, the ASE of the new design of an AM MIMO system for a (2,2) configuration is depicted ($SDCR = 15\,dB, 25\,dB$) and compared to the ASE of the traditional design of an AM MIMO system. It is shown that the ASE of the new design of an AM MIMO system is decreased. Thus, improvement of the BER leads to a lower ASE. The proposed AM mechanism helps to avoid BER degradation by adjusting the spectral efficiency.

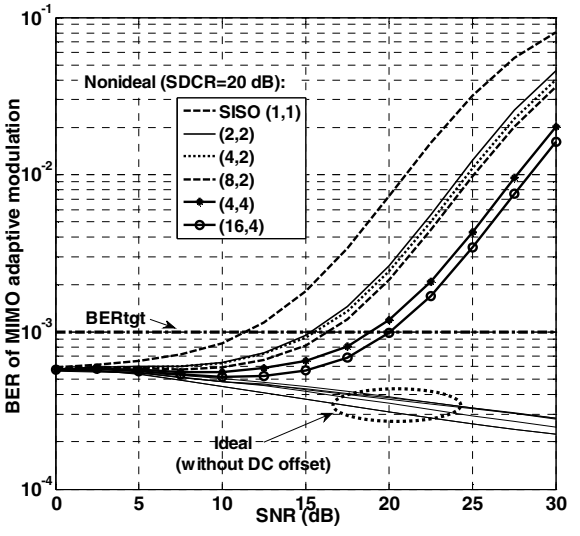

Fig. 9.14 Average BER of AM MIMO systems under the impact of DC offsets (analytic result), $BER_{tgt} = 10^{-3}$, $SDCR = 20\,dB$ $SNR = P/\sigma_w^2$

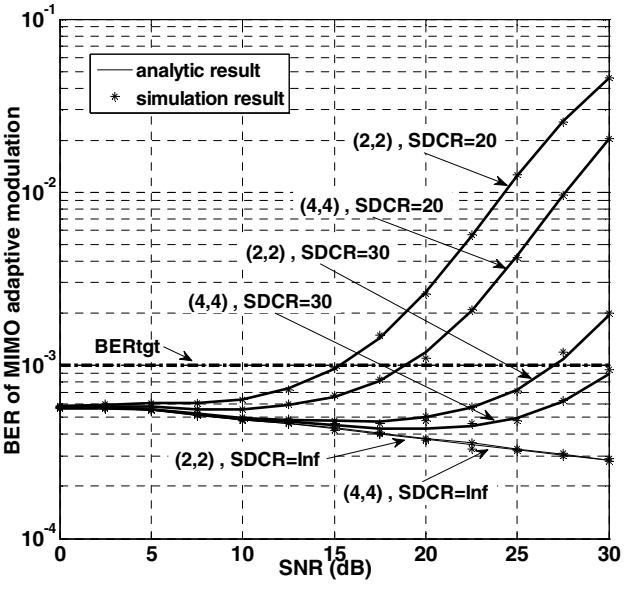

Fig. 9.15 Average BER of AM MIMO systems under the impact of DC offsets under various $SDCR$ values, $BER_{tgt} = 10^{-3}$, $SNR = P/\sigma_w^2$

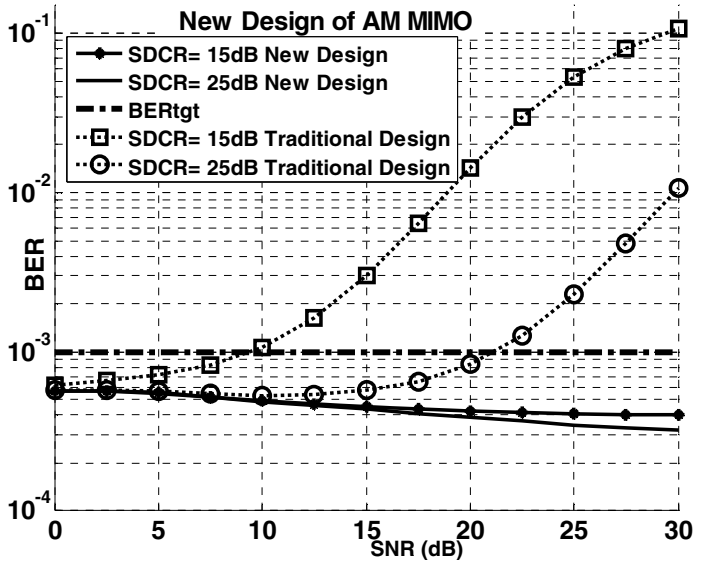

Fig. 9.16 Average BER of a new design of AM MIMO system, $N_t = 2$, $N_r = 2$ $BER_{tgt} = 10^{-3}$, $SNR = P/\sigma_w^2 (2,2)$

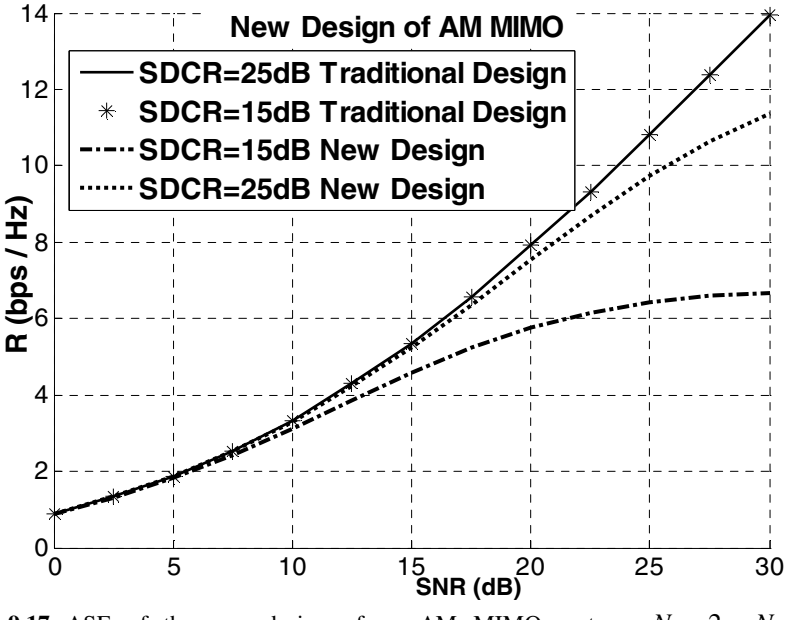

Fig. 9.17 ASE of the new design of an AM MIMO system, $N_t = 2$, $N_r = 2$, $BER_{tgt} = 10^{-3}$, $SNR = P/\sigma_w^2 (2,2)$

The throughput results for the (2,2) configuration are shown in Fig. 9.18. It has been supposed that $R_s = 1 M\,Symbols/S$ and $N_s = 50$. In this figure, the throughput of an AM MIMO system under the impact of a DC offset ($SDCR = 25\,dB$) is compared to the throughput of ideal case (i.e. without DC offset) and the throughput of the new design of an AM MIMO system. As can be seen in this figure, the DC offset degrades the throughput dramatically, and the new design of AM improves it. Due to the BER degradation, the throughput is decreased in the high SNR region. There is an acceptable agreement between simulation results and analytic results in most situations.As may be seen, the difference between the analytical and simulation results is higher with larger SNRs. However, this is predictable, due to the use of larger constellation sizes by the system in higher SNRs. As discussed, the analytical relation only predicts the performance degradation due to the DC offset imperfection.

The imperfections due to the other parameters, such as phase noise and I/Q imbalance, also have impacts that are more noticeable in larger constellation sizes, which correspond to larger SNRs. Accordingly, the difference between the simulation and analytical results will be greater with high SNRs than those with small SNRs.

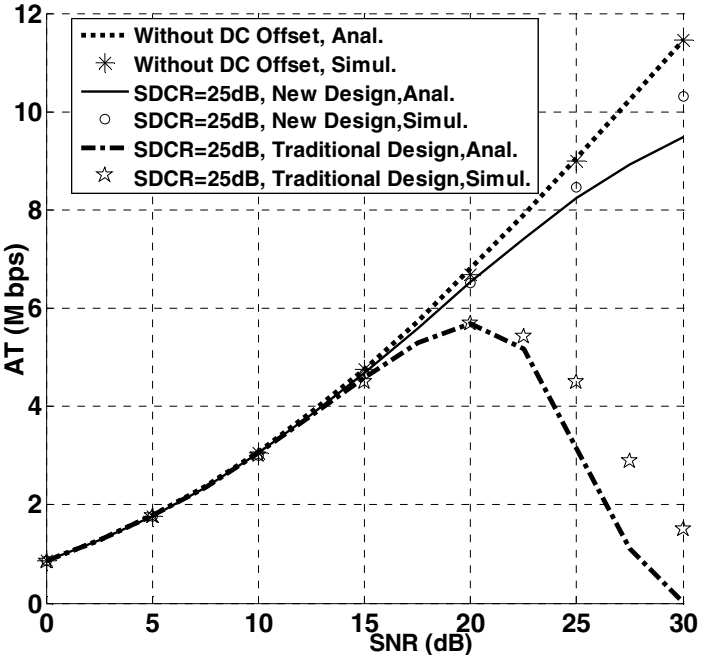

Fig. 9.18 Average throughput of AM MIMO in the presence of DC offset. $N_s = 50$ $R_s = 1 M\,Symbol/S$ $N_t = 2$, $N_r = 2$, $BER_{tgt} = 10^{-3}$, $SNR = P/\sigma_w^2$ (2,2)

The calculated closed form expressions for BER and throughput give us a useful tool to determine whether an ideally designed VRVP AM MIMO system can work in the presence of DC offset.

9.3 I/Q Imbalance in MIMO Transceivers

The I/Q (in-phase/quadrature) imbalance in MIMO systems is also a limiting factor. In this section, the impact of I/Q imbalance on adaptive modulation MQAM MIMO systems is investigated.

9.3.1 I/Q Imbalance Model

The distortion parameters, μ_i and υ_i, are related to the amplitude and phase imbalances between the I and Q branches of each receiving path in the RF/analog demodulation process.

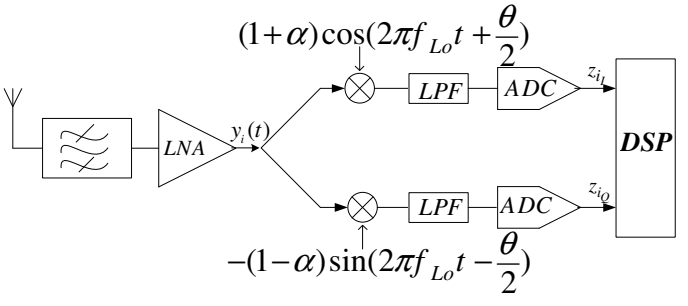

Fig. 9.19 I/Q imbalance in a direct conversion receiver

A simplified model for this distortion is the assumption that there is an amplitude imbalance, α, and a phase imbalance, θ, between the I and Q paths of the mixer, as depicted in Figure 9.19. For such a case, the μ_i and υ_i parameters can be written as [31]:

$$\begin{aligned}\mu &= \cos(\frac{\theta}{2}) + j\alpha\sin(\frac{\theta}{2}) \\ \upsilon &= \alpha\cos(\frac{\theta}{2}) - j\sin(\frac{\theta}{2})\end{aligned} \tag{9.53}$$

9.3.2 MIMO System Model

A flat-fading MIMO channel with N_t transmitting antennas and N_r receiving antennas is considered. Assuming perfect synchronization and perfect channel state information (CSI) at the receiver, the input-output relationship is given by:

$$\mathrm{y}=\mathrm{Hx}+\mathrm{w} \tag{9.54}$$

where y is an $N_r\times1$ vector of the received signal; H denotes the $N_r\times N_t$ channel matrix; x is an $N_t\times1$ vector of the transmitted symbols; and, w is an $N_r\times1$ additive white Gaussian noise (AWGN) vector. The entries of w are also assumed to be independent and $w_i \sim \mathcal{CN}(0,\sigma^2)$. The channel coefficients, $\left\{h_{\mu\upsilon}\right\}_{\mu=1,\upsilon=1}^{N_r,N_t}$, are statistically independent and identically distributed (i.i.d.) complex-valued Gaussian random variables with a variance of 1.

Components of the noise vector have the same distribution with a variance of N_0. The received signal, y, after distortion by I/Q imbalances becomes [32]:

$$\mathrm{z}=\boldsymbol{\mu}\mathrm{y}+\boldsymbol{\upsilon}\mathrm{y}^{*} \tag{9.55}$$

where $\boldsymbol{\mu}=\begin{pmatrix}\mu_1 & 0 & \dots & 0\\ 0 & \mu_2 & \dots & \vdots\\ \vdots & \vdots & \ddots & 0\\ 0 & 0 & \dots & \mu_{N_r}\end{pmatrix}$ and $\boldsymbol{\upsilon}=\begin{pmatrix}\upsilon_1 & 0 & \dots & 0\\ 0 & \upsilon_2 & \dots & \vdots\\ \vdots & \vdots & \ddots & 0\\ 0 & 0 & \dots & \upsilon_{N_r}\end{pmatrix}$.

The distortion parameters, μ_i and υ_i, are related to the amplitude and phase imbalances between the I and Q branches of each receiving path in the RF/analog demodulation process. A simplified model for this distortion is the assumption that there is an amplitude imbalance, α, and a phase imbalance, θ, between the I and Q paths of the mixer, as depicted in Figure 9.20.

For such a case, the μ_i and υ_i parameters can be written as [31]:

$$\begin{aligned}\mu_i &= \cos(\frac{\theta_i}{2}) + j\alpha_i \sin(\frac{\theta_i}{2})\\ \upsilon_i &= \alpha_i \cos(\frac{\theta_i}{2}) - j\sin(\frac{\theta_i}{2})\end{aligned} \tag{9.56}$$

We define $m \overset{\Delta}{=} \min(N_t,N_r)$, $n \overset{\Delta}{=} \max(N_t,N_r)$, $d \overset{\Delta}{=} n-m$. If the singular value decomposition (SVD) is applied to H, it can be expressed as:

$$\mathrm{H}=\mathrm{UDV}^{H} \tag{9.57}$$

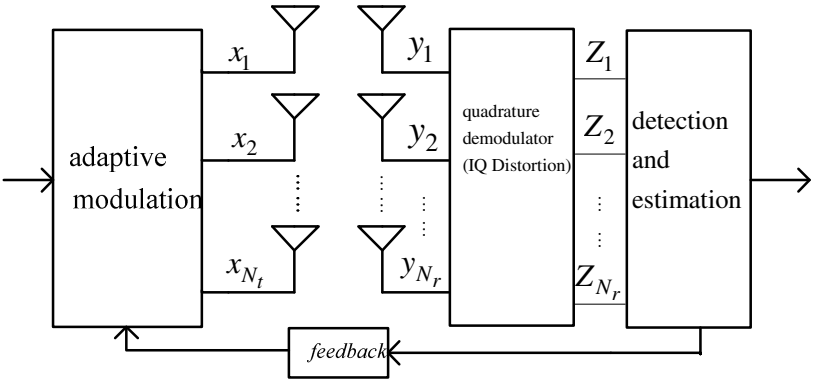

Fig. 9.20 An adaptive modulation MIMO structure

where $(.)^H$ denotes the conjugate transpose; D is an $N_r \times N_t$ matrix with singular values of H, and $\left\{\sqrt{\lambda_i}\right\}_{i=1}^{m}$ are its main diagonal elements; and, U and V are $N_r \times N_r$ and $N_t \times N_t$ unitary matrices with left and right singular vectors of H as their columns, respectively. For the detection and estimation process, the MIMO system should be converted to an m parallel SISO system. Hence, z should be multiplied by U^{H} [33]:

$$\mathrm{z}'=\mathrm{U}^{\mathrm{H}}\mu\mathrm{U}\mathrm{D}\mathbf{x}' + \mathrm{U}^{\mathrm{H}}\upsilon\mathrm{U}^{*}\mathrm{D}\mathbf{x}'^{*} + \mathrm{U}^{\mathrm{H}}\mu\mathbf{w} + \mathrm{U}^{\mathrm{H}}\upsilon\mathbf{w}^{*} \tag{9.58}$$

where $\mathbf{z}' \overset{\Delta}{=} \mathbf{U}^{\mathbf{H}}\mathbf{z}$ and $\mathbf{x}' \overset{\Delta}{=} \mathbf{V}^{\mathbf{H}}\mathbf{x}$. Since U and V are unitary matrices, the powers of x and x' are the same, as well z and z'. If we assume that $\mu' = I - \mu$, where I is the identity matrix; then, (9.58) is written as:

$$\mathrm{z}'=\mathrm{D}\mathbf{x}' - \mathbf{U}^{\mathbf{H}}\boldsymbol{\mu}'\mathbf{U}\mathbf{D}\mathbf{x}' + \mathbf{U}^{\mathbf{H}}\upsilon\mathbf{U}^{*}\mathbf{D}\mathbf{x}'^{*} + \mathbf{U}^{\mathbf{H}}\boldsymbol{\mu}\mathbf{w} + \mathbf{U}^{\mathbf{H}}\upsilon\mathbf{w}^{*} \tag{9.59}$$

Because D is a diagonal matrix, the elements of z' can be written as:

$$z_i' = \sqrt{\lambda_i}\, x_i' + n_{1i}' + n_{2i}' + n_{3i}' \tag{9.60}$$

where $\mathbf{n_1'} = -\mathbf{u_i}^{\mathbf{H}}\boldsymbol{\mu}'\mathbf{U}\mathbf{D}\mathbf{x}' + \mathbf{u_i}^{\mathbf{H}}\upsilon\mathbf{U}^{*}\mathbf{D}\mathbf{x}'^{*}$, $\mathbf{n_2'}=\mathrm{u_i}^{\mathrm{H}}\boldsymbol{\mu}\mathbf{w}$ and $\mathbf{n_3'}=\mathrm{u_i}^{\mathrm{H}}\upsilon\mathbf{w}^{*}$.

From (9.60), we can see that the I/Q imbalance introduces n_{1i}' as the cross channel interference; therefore, the subchannels are no longer parallel. Although in reality the elements of x' usually have values chosen from a set of finite symbols, we assume the entries of $\mathbf{x}'$ are i.i.d. Gaussian variables, i.e. [33]:

$$x_i' \sim \mathcal{CN}(0, \frac{P}{m}) \tag{9.61}$$

where $\frac{P}{m}$ is the average transmitting power constraint of each subchannel. Under this assumption, n' is a zero-mean complex Gaussian random variable with the variance of $\sigma_{n_i'}^2$. We can calculate $\sigma_{n'}^2$ as:

$$\begin{aligned}\sigma_{n_i}'^2 &= E[\mathbf{n_1'n_1'^H}] + E[\mathbf{n_2'n_2'^H}] + E[\mathbf{n_3'n_3'^H}] \\ &= \frac{P}{m}\mathbf{u_i}^{\mathrm{H}}\left(\mu'\mathrm{UDD^H U^H}\mu'^{*} + \boldsymbol{\upsilon}\mathrm{U^*DD^H U^T}\boldsymbol{\upsilon}^{*}\right)u_i + \sigma_w^2\mathbf{u_i}^{\mathrm{H}}\left(\mu\mu^{*} + \boldsymbol{\upsilon}\boldsymbol{\upsilon}^{*}\right)u_i\end{aligned} \tag{9.62}$$

9.3.3 Impact of I/Q Imbalance on BER of Adaptive Modulation MIMO

The BER of an MQAM signal in an AWGN channel can be approximated as:

$$BER(M_i) \simeq \frac{4(1-1/\sqrt{M_i})}{\log_2(M_i)} Q\left(\sqrt{\frac{3\gamma_s}{M_i - 1}}\right) \tag{9.63}$$

where γ_s is the symbol of the received SNR.

As seen, the received signal power (P_{rec}) due to adaptive modulation can be expressed as:

$$P_{rec} = \lambda_1 P_1(\lambda_1) = \frac{-2\ln(5BER_{tgt})\sigma_w^2}{3}(M_i - 1) \tag{9.64}$$

One can approximate the BER of a subchannel by considering (9.63) as:

$$BER_{IQ}(M_i, H) \simeq \frac{4(1-1/\sqrt{M_i})}{\log_2(M_i)} Q\left(\sqrt{\frac{-2\ln(5BER_{tgt})\sigma_w^2}{\sigma_{n'}^2}}\right) \tag{9.65}$$

$BER(M_i, H)$ has the joint pdf of unordered eigenvalues [35]. We can approximate the subchannel BER by averaging the $\sigma_{n'}^2$ using:

$$E_H[\sigma_{n'}^2] = \bar{\lambda}_1 \times \frac{P}{m} u_i^{\mathrm{H}}\left(\mu'\mu'^{*} + \upsilon\upsilon^{*}\right)u_i + \sigma_w^2 u_i^{\mathrm{H}}\left(\mu\mu^{*} + \upsilon\upsilon^{*}\right)u_i \tag{9.66}$$

where $\bar{\lambda}_1 = \int_0^{\infty} \lambda_1 P df_{\lambda_1}(\lambda_1) d\lambda_1$.

If we consider:

$$\Delta = \max\left(\bar{\lambda}_1 \frac{P}{m}(2+\alpha_j^2-2\cos(\tfrac{\theta_j}{2}))+\sigma_w^2(1+\alpha_j^2)\right) \quad j=1,...,N_r \tag{9.67}$$

An approximated upper bound for the BER can then be achieved:

$$BER_{IQ}(M_i) \le \frac{4(1-1/\sqrt{M_i})}{\log_2(M_i)} Q\left(\sqrt{\frac{-2\ln(5BER_{tgt})\sigma_w^2}{\Delta}}\right) \tag{9.68}$$

The average BER of the adaptive modulation MIMO system impaired by I/Q imbalance can be expressed as:

$$BER_{ave} = \frac{\sum_{j=1}^{N} BER_{IQ}(M_j)\times\log_2(M_j)P(\eta_j \le \lambda_1 < \eta_{j+1})}{\sum_{j=1}^{N}\log_2(M_j)P(\eta_j \le \lambda_1 < \eta_{j+1})} \tag{9.69}$$

where $P(\eta_j \le \lambda_1 < \eta_{j+1})$ is the probability that λ_1 falls in the jth region as:

$$p(\eta_j \le \lambda_1 < \eta_{j+1}) = \int_{\eta_j}^{\eta_{j+1}} P df_{\lambda_1}(\lambda_1) d\lambda_1 \tag{9.70}$$

9.3.4 I/Q Imbalance Compensation in Adaptive Modulation MIMO Systems

To compensate for a distorted adaptive modulation MIMO system, adaptation should be done with respect to the I/Q imbalance. In order to obtain the optimal power and rate adaptation for different modulation schemes, we need an expression for the BER in AWGN that is easily inverted, with respect to rate and power. Accordingly, we now introduce a new BER approximation for the MQAM distorted by an I/Q imbalance in AWGN.

From the results of the last section, the following upper bound can be introduced for optimal adaptation as:

$$BER_{IQ}(M) \le 0.2\exp\left(\frac{-1.5\gamma_s}{(M-1)\Delta/\sigma_w^2}\right) \tag{9.71}$$

The values of α and θ are not known at the receiver; therefore, for the implementation of a new adaptation scheme, we use the average of Δ, in terms of α and θ statistics:

$$E[\frac{\Delta}{\sigma_w^2}] = \bar{\lambda}_1 \frac{P}{m\sigma_w^2}(2 + E[\alpha^2 - 2\cos(\frac{\theta}{2})]) + (1 + E[\alpha^2]) \quad (9.72)$$

Based on the definitions of α and θ, $E[\alpha] = E[\theta] = 0$. If we assume a small θ:

$$E[\cos(\frac{\theta}{2})] \simeq 1 - \frac{1}{8}E[\theta^2] \quad (9.73)$$

Accordingly,

$$E[\frac{\Delta}{\sigma_w^2}] = \bar{\lambda}_1 \frac{P}{m\sigma_w^2}(\sigma_\alpha^2 + \frac{1}{4}\sigma_\theta^2) + 1 + \sigma_\alpha^2 \quad (9.74)$$

Now the BER relation is approximated as:

$$BER_{IQ}(M) \le 0.2\exp\left(\frac{-1.5\gamma_s}{(M-1)(\bar{\lambda}_1 \frac{P}{m\sigma_w^2}(\sigma_\alpha^2 + \frac{1}{4}\sigma_\theta^2) + 1 + \sigma_\alpha^2)}\right) \quad (9.75)$$

Based on this approximation, we introduce a new adaptation mechanism as:

$$\begin{cases} k_1(\lambda_1) = r_i, & \eta_i' \le \lambda_1 < \eta_{i+1}' \\ P_1(\lambda_1) = \dfrac{M_i - 1}{\lambda_1}\dfrac{\sigma_w^2}{K}CF, & \eta_i' \le \lambda_1 < \eta_{i+1}' \end{cases} \quad (9.76)$$

where the compensation factor (CF) is defined as:

$$CF = \bar{\lambda}_1 \frac{P}{m\sigma_w^2}(\sigma_\alpha^2 + \frac{1}{4}\sigma_\theta^2) + 1 + \sigma_\alpha^2 \quad (9.77)$$

and $\eta_i' = \frac{M_i - M_{i-1}}{r_i - r_{i-1}}\frac{\mu}{K}CF$.

The Lagrangian multiplier, β, is calculated as:

$$\sum_{i=1}^{N} \frac{M_i - 1}{K}\left[\int_{\eta_i'}^{\infty} \frac{Pdf_{\lambda_1}(\lambda_1)}{\lambda_1} d\lambda_1 - \int_{\eta_{i+1}'}^{\infty} \frac{Pdf_{\lambda_1}(\lambda_1)}{\lambda_1} d\lambda_1\right] = \frac{P}{m\sigma_w^2 CF} \quad (9.78)$$

and the ASE is calculated as:

$$R = m\sum_{i=1}^{N} r_i\left[\int_{\eta_i'}^{\infty} Pdf_{\lambda_1}(\lambda_1)d\lambda_1 - \int_{\eta_{i+1}'}^{\infty} Pdf_{\lambda_1}(\lambda_1)d\lambda_1\right] \quad (9.79)$$

9.3.5 BER Analysis

In this section, an experimental study is presented; and, the analytical relations are compared with measurement results. The effect of an I/Q imbalance (for two sets of phase and amplitude errors) on the BER of adaptive modulation MIMO is depicted in Figure 9.21. The BER of an ideal adaptive modulation MIMO is also illustrated in this figure. The comparison between the ideal and impaired systems shows the extreme degradation of the adaptive MIMO system due to the I/Q imbalance. Good agreement between the measurement results and the simulation results can be observed in this figure. It can be seen that the approximated analytic BER upper bound follows the simulation and measurement results very well. The impact of different parameters on BER is determined from this analytic expression. Figure 9.21, however, shows an unusual behavior: by increasing the average SNR, the BER became more degraded. This response is expected, because the adaptive modulator uses high-order components, which are more sensitive to I/Q imbalance, in the modulation of high SNR regions.

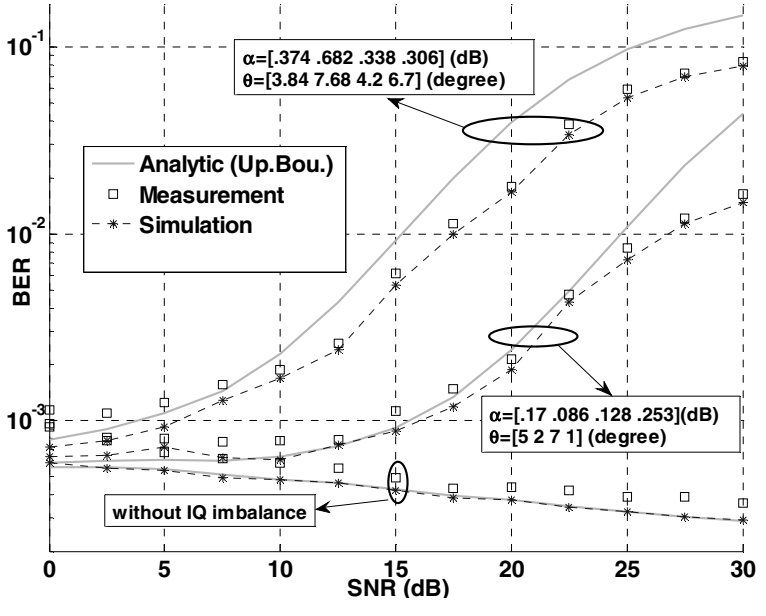

Fig. 9.21 BER of an adaptive modulation MIMO system with I/Q imbalance

Figure 9.22 (top) shows the BER of an adaptive modulation MIMO system impaired by an I/Q imbalance before and after the compensation operation by supposing $\sigma_\alpha = 0.3dB$ and $\sigma_\theta = 5^\circ$.

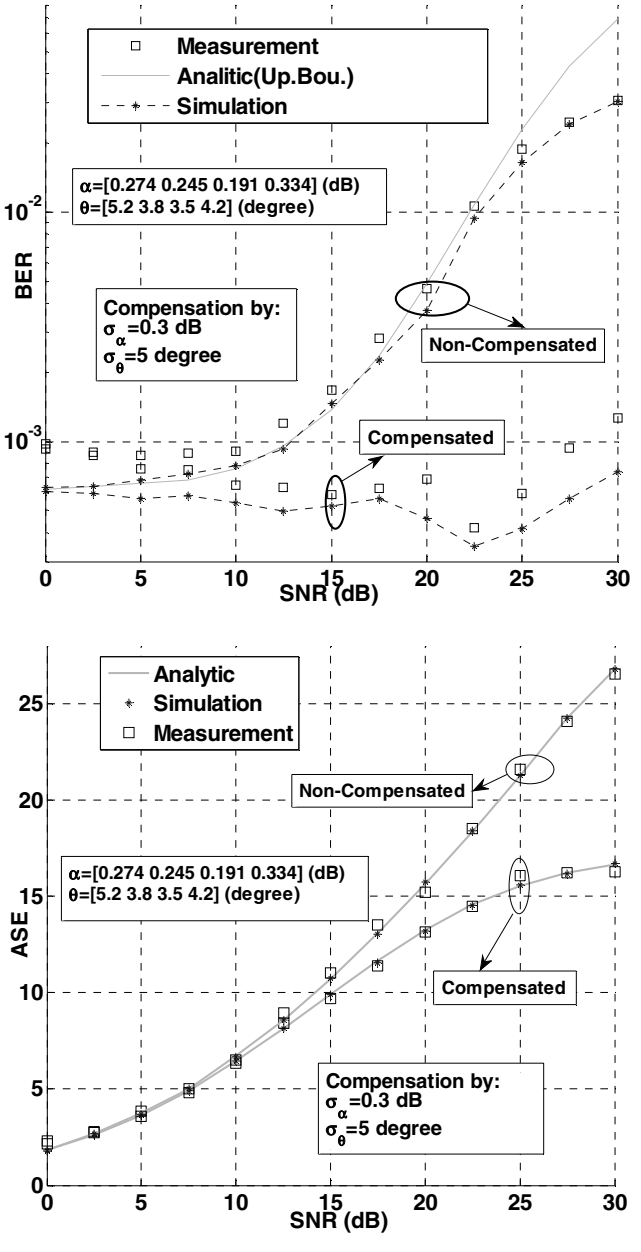

Fig. 9.22 (Top) BER of an I/Q imbalance compensated adaptive modulation MIMO system, and (bottom) ASE of an I/Q imbalance compensated adaptive modulation MIMO system

References

[1] Paulraj, A., Nabar, R., Gore, D.: Introduction to Space-Time Wireless Communications. Cambridge University Press (2003)
[2] Bolcskei, H., Gesbert, D., Papadias, C.B., Veen, A.: Space-Time Wireless System From Array Processing to MIMO Communications. Cambridge University Press (2006)
[3] Schenk, T., Linnartz, J.: RF Imperfections in High-Rate Wireless Systems, Impact and Digital Compensation. Springer, Heidelberg (2008)
[4] Piazzo, L., Mandarini, P.: Analysis of phase noise effects in OFDM modems. IEEE Transactions on Communications 50(10), 1696–1705 (2002)
[5] Tomba, L.: On the effect of wiener phase noise in OFDM systems. IEEE Transactions on Communications 46(5), 580–583 (1998)
[6] Howald, R., Kesler, S., Kam, M.: BER performance of MQAM using OFDM with RF carrier phase noise. In: Proceedings of Southeastern Symposium on System Theory, pp. 419–423 (1998)
[7] Liu, P., Bar-Ness, Y.: Closed-form expressions for BER performance in OFDM systems with phase noise. In: Proceedings of International Conference on Communications (ICC), Turkey, pp. 5366–5370 (2006)
[8] Lu, J., Letaief, K.B., Chuang, J., Liou, M.L.: M-PSK and M-QAM BER computation using signal-space concepts. IEEE Transactions on Communications 47(2), 181–184 (1999)
[9] Proakis, J.G., Salehi, M.: Digital Communications, 5th edn. McGraw-Hill (2007)
[10] Dohler, M.: Virtual antenna arrays, Ph.D. dissertation, King's College, London, U.K (2003)
[11] Chung, S.T., Goldsmith, A.J.: Degrees of freedom in adaptive modulation: A unified view. IEEE Transactions on Communications 49(9), 1561–1571 (2001)
[12] Keshavarzi, M.R., Mohammadi, A., Abdipour, A.: Characterization of Adaptive Modulation MIMO Systems in the Presence of Phase Noise. In: International Conference on Wireless Communications & Mobile Computing, IWCMC, Leipzig, Germany, pp. 1243–1247 (2009)
[13] Muschallik, C.: Influence of RF oscillators on an OFDM signal. IEEE Transactions on Consumer Electronics 41, 592–603 (1995)
[14] Gershman, A.B., Sidiropoulos, N.D.: Space-Time Processing for MIMO Communications. Wiley (2005)
[15] Tsoulos, G.: MIMO System Technology for Wireless Communications. CRC Press (2006)
[16] Zhou, S., Giannakis, G.B.: How accurate channel prediction needs to be for transmit-beamforming with adaptive modulation over Rayleigh MIMO channels? IEEE Transactions on Wireless Communications 3(4), 1285–1294 (2004)
[17] Leung, B.: VLSI for Wireless Communications. Prentice Hall (2002)
[18] Hemesi, H., Azami, F., Ghorssi, A., Abdipour, A., Mohammadi, A.: Low-complexity channel and frequency offset estimation in MIMO systems. Electronic Letters 44(9), 599–600 (2008)
[19] Larson, E.: RF and Microwave Circuit Design for Wireless Communications. Artech House, Norwood (1996)

[20] Bateman, A., Haines, D.M.: Direct conversion transceiver design for compact low-cost portable mobile radio terminals. In: Proceedings of the 43th IEEE Vehicular Technology Conference, pp. 55–62 (1989)
[21] Keshavarzi, M.R., Mohammadi, A., Abdipour, A., Ghannouchi, F.M.: Characterization and Compensation of DC Offset on Adaptive MIMO Direct Conversion Transceivers. IEICE Transactions on Communications (1), 253–261 (2011)
[22] Kenington, P.B.: RF and Baseband Techniques for Software Defined Radio. Artech House, Norwood (2005)
[23] Lindoff, B., Malm, P.: BER performance analysis of a direct conversion receiver. IEEE Transactions on Communications 50(5), 856–865 (2002)
[24] Lu, J., Letaief, K.B., Chuang, J.C.-I., Liou, M.L.: M-PSK and M-QAM BER Computation Using Signal-Space Concepts. IEEE Transactions on Communications 47, 181–184 (1999)
[25] Proakis, J.G., Salehi, M.: Digital Communications, 5th edn. McGraw-Hill (2007)
[26] Mohammadi, A., Kumar, S.: Characterization of adaptive modulators in fixed wireless ATM networks. KICS/IEEE Journal of Communications and Networks 6(2), 123–132 (2004)
[27] Dohler, M., Aghvami, H.: On the approximation of MIMO capacity. IEEE Transactions on Wireless Communications 4(1), 30–34 (2005)
[28] Zhou, Z., Vucetic, B., Dohler, M., Li, Y.: MIMO systems with adaptive modulation. IEEE Transactions on Vehicular Technology 54(5), 1828–1842 (2005)
[29] Goldsmith, A.: Wireless Communications. Cambridge University Press (2005)
[30] Pursley, M.B., Shea, J.M.: Adaptive nonuniform phase-shift-key modulation for multimedia traffic in wireless networks. IEEE Journal on Selected Areas in Communications 18, 1394–1407 (2000)
[31] Liu, C.L.: Impacts of I/Q imbalance on QPSK-OFDM-QAM detection. IEEE Transactions on Consumer Electronics 44(3), 984–989 (1998)
[32] Tarighat, A., Sayed, A.H.: MIMO OFDM receivers for systems with IQ imbalances. IEEE Transactions on Signal Processing 53(9), 3583–3596 (2005)
[33] Zhou, Z., Vucetic, B., Dohler, M., Li, Y.: MIMO systems with adaptive modulation. IEEE Transactions on Vehicular Technology 54(5), 1828–1842 (2005)
[34] Dohler, M.: Virtual antenna arrays, Ph.D. dissertation, King's College, London (2003)
[35] Telatar, I.E.: Capacity of multi-antenna Gaussian channels. European Transactions on Telecommunications 10, 585–595 (1999)
[36] Hemesi, H., Azami, F., Ghorssi, A., Mohammadi, A., Abdipour, A.: Design and Implementation of a Flexible 4x4 MIMO Testbed. In: Proceedings of the International Symposium on Telecommunications (IST 2008), pp. 266–272 (2008)